Arabian Journal of Chemistry (2014) 7, 71–77

King Saud University

Arabian Journal of Chemistry

www.ksu.edu.sa
www.sciencedirect.com

SPECIAL ISSUE: ENVIRONMENTAL CHEMISTRY

# Photocatalytic decomposition of dyes using ZnO doped $SnO_2$ nanoparticles prepared by solvothermal method

**Mohamed M. Rashad [a], Adel A. Ismail [a,*], I. Osama [a], I.A. Ibrahim [a], Abdel-Hakim T. Kandil [b]**

[a] *Central Metallurgical Research & Development Institute (CMRDI), P.O. Box 87, Helwan 11421, Egypt*
[b] *Department of Chemistry, Faculty of Science, Helwan University, Cairo, Egypt*

Received 4 July 2013; accepted 16 August 2013
Available online 25 August 2013

**KEYWORDS**

ZnO;
Doping;
Stannic oxide;
Solvothermal method;
Photocatalysis

**Abstract** ZnO doped $SnO_2$ has been successfully synthesized by the solvothermal method using methanol as organic solvent. The effect of ZnO/$SnO_2$ molar ratios on the crystal structure, microstructure, optical and photocatalytic properties has been investigated. The synthesized samples are characterized by X-ray diffraction, transmission electron microscopy, $N_2$ physical adsorption, FT-IR spectroscopy and UV–Vis spectroscopy. XRD results revealed that all diffraction peaks positions agree well with the reflection of a tetragonal rutile structure of $SnO_2$ phase without extra peaks at 0.1ZnO:0.9$SnO_2$ and 0.2ZnO:0.8$SnO_2$ molar ratios. However, the secondary phase of ZnO at 0.3ZnO:0.7$SnO_2$ molar ratio was investigated. TEM images revealed that the shape of $SnO_2$ particles was spherical and the particle sizes of $SnO_2$ and 0.3ZnO:0.7$SnO_2$ molar ratio were 6.2 and 16.4 nm, respectively. The newly prepared samples have been tested by the determination of photocatalytic degradation of methylene blue (MB). The results indicated that $Zn^{2+}$ doping at 0.3ZnO:0.7 $SnO_2$ molar ratio showed the highest photocatalytic activity for the MB photodegradation. The heightened photocatalytic activity of ZnO/$SnO_2$ could be ascribed to the enhanced charge separation derived from the coupling of ZnO with $SnO_2$ due to the potential energy differences between $SnO_2$ and ZnO. The recycling tests demonstrated that 0.3ZnO:0.7 $SnO_2$ photocatalysts were quite stable during that liquid–solid heterogeneous photocatalysis since no decrease in activity in the first four cycles was observed.

© 2013 Production and hosting by Elsevier B.V. on behalf of King Saud University.

## 1. Introduction

There has been extensive interest in developing semiconductor photocatalysts with high activities for environmental applications such as air purification, water disinfection, hazardous waste remediation, and water purification (Hoffmann et al., 1995; Fujishima et al., 2000; Kormann et al., 1991; Zhang et al., 2005; Ismail, 2008; Kostedt et al., 2008). The

* Corresponding author. Tel./fax: +20 2 25010643.
E-mail address: aismail@cmrdi.sci.eg (A.A. Ismail).
Peer review under responsibility of King Saud University.

Production and hosting by Elsevier

1878-5352 © 2013 Production and hosting by Elsevier B.V. on behalf of King Saud University.
http://dx.doi.org/10.1016/j.arabjc.2013.08.016

photochemistry of semiconductor nanoparticles and nanoparticulate materials is a fast growing area, both in terms of research and commercial activity (Brokken-Zijp et al., 2011; Mills and Lee, 2002). A photocatalytic process is based on the generation of electron–hole pairs by means of band-gap radiation that can give rise to redox reactions with the species adsorbed on the surface of the photocatalysts (Wang et al., 2005; Yuan and Xu, 2010). However, the high degree of recombination of photogenerated electrons and holes in semiconductors decreased greatly their photocatalytic efficiency and impeded the practical application of the photocatalytic technique in the degradation of contaminants in water and air. Thus, a major challenge in photocatalysis is the need to increase the charge separation efficiency of the photocatalyst and its photocatalytic efficiency. Fortunately, the doping semiconductor particles with difference in band-gap energy could increase the charge separation and extend the energy range of photoexcitation, so doping semiconductor photocatalysts exhibited higher photocatalytic activity for both gas- and liquid-phase reactions than single semiconductor photocatalysts (Pal et al., 2001; Yu et al., 1998; Ismail and Bouzid, 2013; Mahamoud et al., 2012; Lin and Chiang, 2012). ZnO, $TiO_2$ and $SnO_2$ have been recognized to be preferable materials for photocatalytic processes due to their high photo-sensitivity, low cost and chemical stability. However, the band gap energy of $TiO_2$ (3.2 eV), ZnO (3.3 eV) and $SnO_2$ (3.6 eV) limits the absorption ability of the high-energy portion (UV) of the sunlight, which results in relatively small efficiency (Fouad et al., 2006; Ismail et al., 2010; Vinodgopal et al., 1996). $SnO_2$ is particularly interesting because it has outstanding optical, electrical and mechanical properties, is a versatile material and is widely used as the most attractive material for gas sensor applications, as a catalyst during the oxidation of organic compounds, as a key component in rechargeable Li batteries, and as a master element in opto-electronic devices (Borges et al., 2010; Zheng et al., 2007). A number of preparations of $SnO_2$ nanoparticles by methods such as co-precipitation (Rumyantseva et al., 2005), sol–gel method (Broussous et al., 2002; Gu et al., 2003; Kotsikau et al., 2004), solvothermal (Sathyaseelan et al., 2010), chemical vapor deposition (Suh et al., 1999; Huh et al., 1999), VLS method (He et al., 2006), laser ablation(Monredon et al., 2002) and hydrothermal method (Firooz et al., 2008) have been developed. Among these methods, solvothermal method is well suited for the production of nanostructure materials, because of its relatively low processing cost, being much milder and the ability to control the grain size (Anandan and Rajendran, 2010). In this study, ZnO doped $SnO_2$ at different molar ratios has been successfully synthesized by the solvothermal method using methanol as organic solvent. The newly prepared samples have been tested by the determination of photocatalytic degradation of MB. The latter compound was used because it exhibits a high molar absorptivity (or molar extinction coefficient) allowing the rate of bleaching to be readily evaluated.

## 2. Experimental section

### 2.1. Chemicals and materials

Chemically grade $SnCl_4{\cdot}5H_2O$, $Zn(CH_3COO)_2$ and methanol were purchased from Sigma–Aldrich and used as the starting materials for $SnO_2$ and ZnO, whereas NaOH was purchased from Fluka.

### 2.2. Procedure

#### 2.2.1. Preparation of $ZnO/SnO_2$ nanoparticles

A stoichiometric amount of $SnCl_4{\cdot}5H_2O$ and $Zn(CH_3COO)_2$ was dissolved in 300 ml methanol. 5 M sodium hydroxide solution was obtained by dissolving it in methanol then added to the above solution. It was employed as a base to attain the pH = 7 for complete precipitation of Zn. The resulting solutions were poured into a stainless Telfon-lined 100 ml capacity autoclave. The autoclave was sealed and heated to maintain at 150 °C for 6 h, and then air-cooled to room temperature. The precipitates were repeatedly washed with deionized water and absolute methanol then dried at 80 °C for 24 h. The formed powder was annealed at 800 °C for 30 min to get crystalline powders using a tube furnace in static atmosphere.

### 2.3. Physical characterization

The crystallite phases of different annealed samples identified by X-ray diffraction (XRD) using a Brucker axis D8 diffractometer with crystallographic data software Topas 2 using Cu-K$\alpha$ radiation. The crystallite size of undoped and doped stannic oxide nanoparticles was quantitatively determined based on Scherrer's formula, further most intense peak of the $SnO_2$ phase. The particles morphology was observed using Transmission electron microscopy (TEM) recorded with a JEOL-JEM-1230 microscope. The UV–Vis absorption spectrum was recorded by a UV–Vis–NIR scanning spectrophotometer (Jasco-V-570 Spectrophotometer, Japan) using a 1 cm path length quartz cell. UV–Vis spectra were detected in the diffuse reflectance mode (R) and transformed to the Kubelka–Munk function $F(R)$ to separate the extent of light absorption from scattering. Furthermore the band gap values were obtained from the plot of the modified Kubelka–Munk function $(F(R)\ E)^2$ versus the energy of the absorbed light $E$ (Tauc et al., 1966; Ismail et al., 2012).The band gap energy was determined from the intersection of tangent through the point of inflection in the absorption band and the photon energy axis. Fourier transforms infrared spectrometer (FT-IR; JASCO, Model 6300) spectrum was recorded in KBr dispersion in the range of 400–4000 $cm^{-1}$.

### 2.4. Photocatalytic activity tests

The photocatalytic tests were performed in an aqueous solution using MB ($C_{16}H_{18}ClN_3S$) (Aldrich, $\lambda_{max}$ = 664 nm) as the probe molecule. A quartz photoreactor was filled with 250 $cm^3$ aqueous solution of MB at a concentration of $10^{-5}$ M (3.198 ppm) and mixed with 0.1 g of newly prepared photocatalysts. UV irradiation was performed by a 150 W medium pressure xenon lamp (Osram) immersed in a quartz jacket and equipped with a cooling tube. This lamp provides a relatively continuous light output from 250 to 700 nm, with a number of sharp lines occurring near 450 nm and above 800 nm. The lamp was switched on 30 min prior to the start of the reaction to stabilize the power of its emission and the reactor was cooled by circulation of $H_2O$. The temperature of the cooling water was stabilized to perform the reactions

at 25 °C. The concentration of the substrate after equilibration was measured and taken as the initial concentration ($C_0$) to discount the adsorption in the dark. MB samples were withdrawn at regular intervals ($C$) from the upper part of the reactor with the catalyst being removed from the liquid phase by filtration through nylon syringe filters (pore size: 0.45 μm). The photodegradation rate was determined by measuring the MB remaining in the aqueous solution through 3 h of illumination. Measurements were carried out using JASCO V-570 UV–Vis spectrophotometer.

## 3. Results and discussion

### 3.1. Structural studies

Fig. 1 represents the XRD patterns of undoped $SnO_2$ and 0.1ZnO:0.9$SnO_2$, 0.2ZnO:0.8$SnO_2$ and 0.3ZnO:0.7$SnO_2$ molar ratios. It is clear that peak positions agree well with the reflection of tetragonal rutile structure of the $SnO_2$ phase (JCPDS#72-1147). Furthermore, there are no extra peaks of ZnO at 0.1ZnO:0.9$SnO_2$ and 0.2ZnO:0.8$SnO_2$ molar ratios where the diffraction peaks arise at (110), (101), (200), (111), (211), (220) and (002) without any other phases detected indicating that Zn ions were embedded into the crystal lattice of $SnO_2$. Also, the results indicate that Zn ions get substituted at the Sn site without changing the cassiterite structure. However, secondary phase of hexagonal ZnO was detected at 0.3ZnO:0.7$SnO_2$ molar ratio (Ismail et al., 2005) (JCPDS#79-2205). It is observed that the peak position shifts to higher 2$\theta$ as the ZnO molar ratio increases. Table 1 summarize the variation of the crystallite size and the change in lattice parameters calculated from the (110) and (101) peaks of undoped $SnO_2$ and Zn doped $SnO_2$. The results indicated that the lattice parameters, unit cell volume and the crystallite size were decreased with increasing Zn substitution ratio (Table 1).

Fig. 2 shows the TEM images of undoped $SnO_2$ (Fig. 2a) and 0.3ZnO:0.7$SnO_2$ (Fig. 2b) molar ratio. It revealed that the shape of $SnO_2$ particles were spherical and agglomerated (Fig. 2a). Zn substituted $SnO_2$ had reduced the agglomeration degree of the undoped sample and the shape of Zn substituted $SnO_2$ particles was nearly spherical and cubical indicating the presence of a second phase (Fig. 2b). These micrographs show that the particle sizes of $SnO_2$ and 0.3ZnO:0.7$SnO_2$ molar ratio samples were 6.2 and 16.4 nm, respectively which was in agreement with the crystallite size calculated XRD analysis as you see in Table 1.

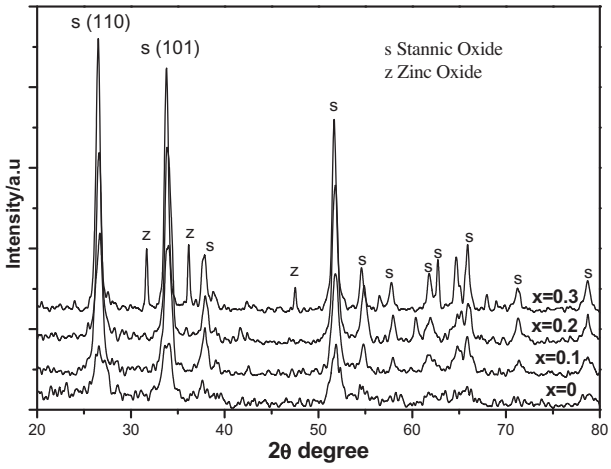


**Figure 1** XRD patterns of undoped $SnO_2$ and 0.1ZnO:0.9$SnO_2$, 0.2ZnO:0.8$SnO_2$ and 0.3ZnO:0.7$SnO_2$ molar ratios.

Fig. 3 showed FTIR spectra of undoped $SnO_2$ and 0.3ZnO:0.7$SnO_2$ molar ratio samples within 400–4000 $cm^{-1}$. The results revealed that the peak at 3438 $cm^{-1}$ comes from the stretching mode vibrations of OH, while the peak at 1636 $cm^{-1}$ is attributed to the bending vibrations of adsorbed $H_2O$ molecules. The small peak at 1364 $cm^{-1}$ is due to the bending vibrations of C–H in the methyl which maybe comes from the residues of preparation processes. It indicates that there may be a very small amount of organic residues in the $SnO_2$ and ZnO nanoparticles. Also, the strong peak at 615 $cm^{-1}$ can be ascribed to the vibration of Sn–O bond in $SnO_2$ as shown in the literature (Dutta and De, 2007; Zhong and Liu, 1999; Monredon et al., 2002).

UV–Vis spectroscopy was performed on all samples (undoped $SnO_2$ and 0.1ZnO:0.9$SnO_2$, 0.2ZnO:0.8$SnO_2$ and 0.3ZnO:0.7$SnO_2$ molar ratios) to observe the change in optical properties of the formed $SnO_2$ as a function of Zn substitution. The transmittance edge of ZnO/$SnO_2$ samples varies as the content of Zn ions in $SnO_2$ nanoparticles varies. They show a slight red shift in the band transition from the normal value with adding the ZnO dopant at 0.3ZnO:0.7$SnO_2$ molar ratio (Fig. 4). The optical band gap is calculated from plotting $(\alpha h\upsilon)^n$ versus $h\upsilon$ and a direct transition is found for undoped and substituted $SnO_2$ nanoparticles. The data are summarized in Table 1. The calculated band gap of undoped $SnO_2$ nanoparticles was found to be 3.75 eV, which is higher than the reported value of the bulk $SnO_2$ i.e. 3.6 eV (Sharma et al., 2011; Fang et al., 2008). The band gaps of 0.1ZnO:0.9$SnO_2$, 0.2ZnO:0.8$SnO_2$ and 0.3ZnO:0.7$SnO_2$ photocatalysts estimated from the tangent lines are 3.61, 3.56, and 3.33 eV, respectively. These values are all in the range of experimental error (±0.1 eV) (Table 1). The appearance of such larger band gap energy is expected in $SnO_2$ nanoparticles because of their small size ~6 nm.

### 3.2. Photocatalytic properties

When the ZnO/$SnO_2$ catalyst is radiated by UV light with photon energy higher or equal to the band gaps of $SnO_2$ and ZnO, electrons ($e^-$) in the VB can be excited to the CB with simultaneous generation of the same amount of holes ($h^+$) in the VB. The photogenerated electrons and holes are separated under the influence of the electrostatic field induced by different work functions. Thus, electrons move to the $SnO_2$ side and holes to the ZnO side. The photogenerated electrons and holes in the ZnO/$SnO_2$ heterojunction nanocatalyst could inject into a reaction medium and participate in chemical reactions (Zheng et al., 2009). The hole in the valence band can react with $H_2O$ or hydroxide ions adsorbed at the particle surface to produce hydroxyl radicals (OH**.**), while the electron in the conduction band can reduce $O_2$ to produce superoxide radicals ($O_2$**.**$^-$) and subsequently other reactive oxygen species (i.e., $H_2O_2$ and OH**.**). Both, holes and OH**.** are extremely reactive toward organic compounds (Hoffmann et al., 1995; Ismail and Bahnemann, 2011). The time-dependent UV–Vis spectra of MB during the irradiation under UV light with different catalytic materials

**Table 1** Variation of crystal size, lattice parameters, cell volume and band gap energy of undoped $SnO_2$ and $ZnO:SnO_2$ at different molar ratios.

| Sample | Cs (nm) | $a = b$ (Å) | $c$ (Å) | Cell volume | BG (eV) |
|---|---|---|---|---|---|
| $SnO_2$ | 5.5 | 4.75 | 3.19 | 71.565 | 3.75 |
| $0.1ZnO:0.9SnO_2$ | 13.7 | 4.73 | 3.18 | 71.154 | 3.61 |
| $0.2ZnO:0.8SnO_2$ | 13.9 | 4.74 | 3.18 | 71.394 | 3.56 |
| $0.3ZnO:0.7SnO_2$ | 18.7 | 4.74 | 3.19 | 71.115 | 3.33 |

Cs, crystallite size, BG, bandgap energy.

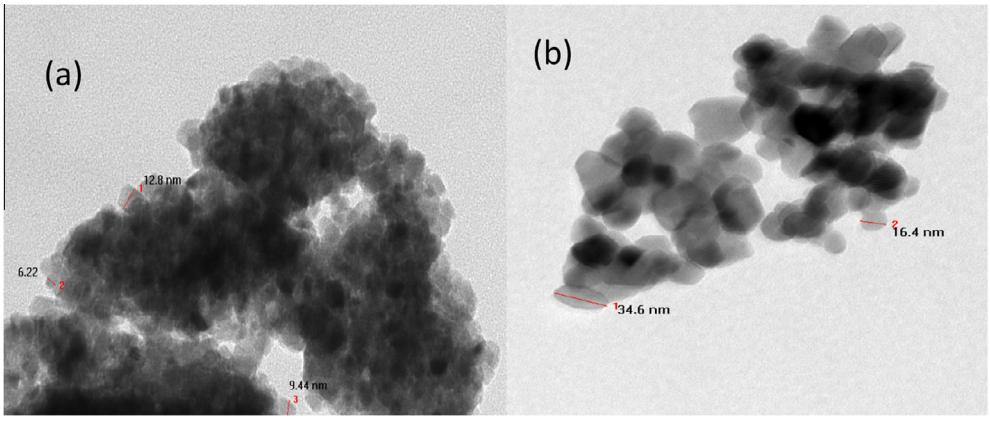


**Figure 2** TEM images of (a) undoped $SnO_2$ and (b) $0.3ZnO:0.7SnO_2$ molar ratio.

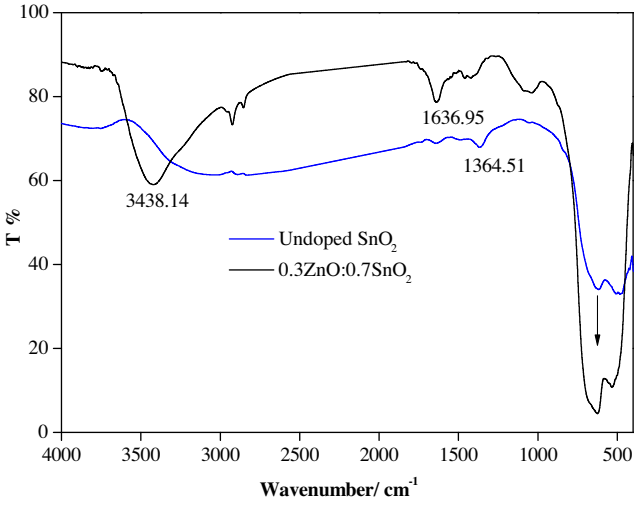


**Figure 3** FTIR spectra for undoped $SnO_2$ and $0.3ZnO:0.7SnO_2$ molar ratio.

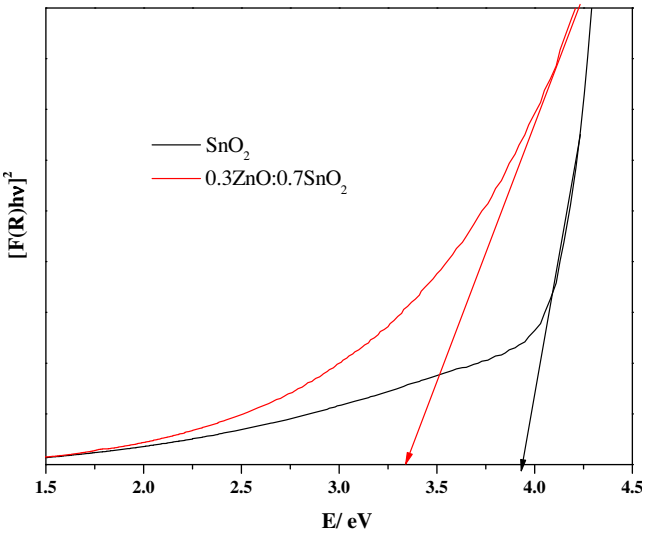


**Figure 4** Plot of transferred Kubelka–Munk versus energy of the light absorbed of the undoped $SnO_2$ and $0.3ZnO:0.7SnO_2$ molar ratio.

are shown in Fig. 5. It can be observed that the maximum absorbance of 664 nm decreases gradually according to the photocatalysts after 240 min. The photocatalytic degradation of MB was carried out using the newly prepared photocatalysts, undoped $SnO_2$ and $0.3ZnO:0.7SnO_2$ molar ratio (Fig. 5a and b). It is clearly seen that, the strong absorption bands of MB those that are located at $\lambda = 290$ nm and $\lambda = 664$ nm steadily decrease upon increasing irradiation times. The photocatalytic activity improved significantly in the presence of $Zn^{2+}$ doping showing the highest photocatalytic activity for the MB decoloration where the absorbance at $\lambda_{max} = 664$ nm decreased from 0.75 to 0.15 after nearly 240 min of irradiation using $0.3ZnO:0.7SnO_2$ sample (Fig. 5b). The enhancement in the photocatalytic activity may come from the hetero-junctions of the $ZnO/SnO_2$ photocatalyst, its surface area and its dispersion in solution. The photocatalytic activities of the undoped either $SnO_2$ or ZnO and $ZnO/SnO_2$ samples at different molar ratios for the degradations of MB were illustrated in Fig. 6. The photocata-

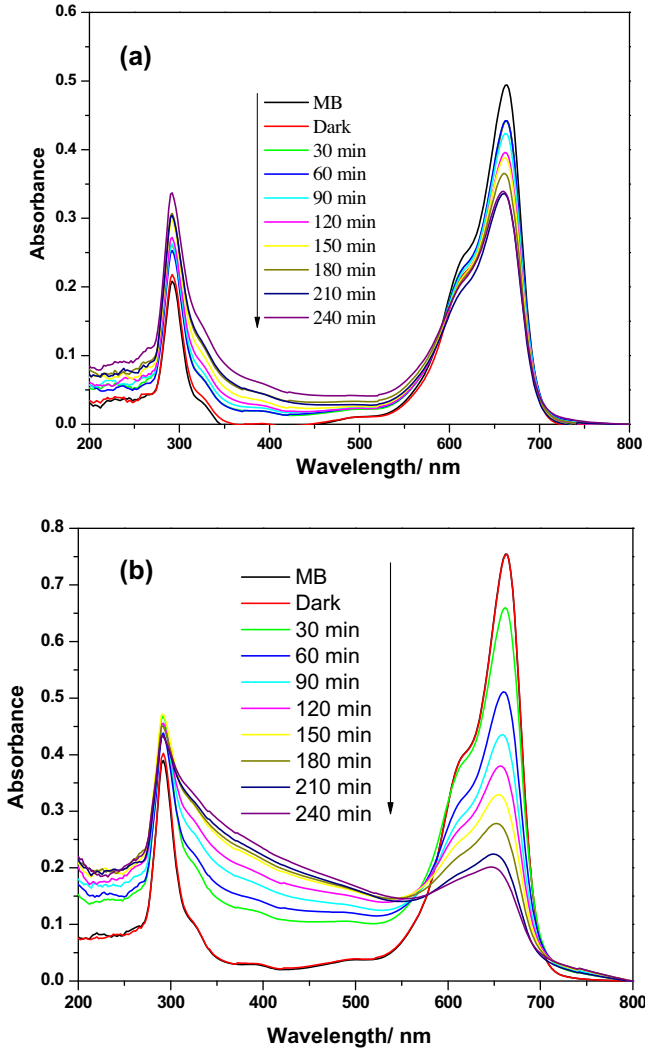


**Figure 5** The absorbance spectra changes of MB solution in undoped $SnO_2$ (a) and 0.3ZnO:0.7$SnO_2$ molar ratio (b).

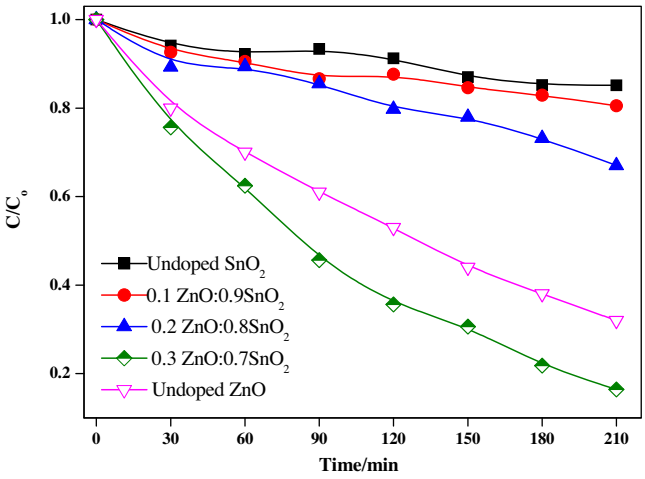


**Figure 6** Photocatalytic decolorization kinetics of MB using either undoped $SnO_2$ or ZnO, 0.1ZnO:0.9$SnO_2$, 0.2ZnO:0.8$SnO_2$ and 0.3ZnO:0.7$SnO_2$ molar ratios. (MB concentration [$10^{-5}$ M], volume 250 ml.)

lytic activities of the Zn doped $SnO_2$ photocatalysts change with the Zn contents, photocatalysts with 0.1ZnO:0.9$SnO_2$, 0.2ZnO:0.8$SnO_2$ and 0.3ZnO:0.7$SnO_2$ molar ratios show higher photocatalytic activities than undoped $SnO_2$ (Fig. 6). Also, the decrease of $SnO_2$ content led to increase in the photocatalytic activity of the doped photocatalyst because of the very low photocatalytic activity of $SnO_2$. On the other hand, the photoactivity of undoped ZnO photocatalysts is higher than undoped $SnO_2$, however, photocatalyst with 0.3ZnO:0.7$SnO_2$ molar ratio is much better than either undoped $SnO_2$ or ZnO. This may be due to the formation of hetero-junctions between ZnO, $SnO_2$ and $Zn_2SnO_4$ (Lin and Chiang, 2012; Sathyaseelan et al., 2010; Firooz et al., 2008; Tennakone and Bandara, 2001). The heightened photocatalytic activity of ZnO/$SnO_2$ could be further ascribed to the enhanced charge separation derived from the coupling of ZnO with $SnO_2$ due to the potential energy differences between $SnO_2$ and ZnO, which would promote interfacial charge-transfer relative to that of charge carrier recombination (Dodd et al., 2006; Zheng et al., 2009) thus enhancing the photocatalytic activity. The order of photocatalytic activity of Zn doped $SnO_2$ at 210 min was as follows: 0.3ZnO:0.7$SnO_2$ > ZnO:0.8$SnO_2$ > 0.1ZnO:0.9$SnO_2$, which suggested that the $Zn^{2+}$ doping enhanced the photocatalytic activity of $SnO_2$. The 0.3ZnO:0.7$SnO_2$ photocatalyst exhibited the highest photocatalytic efficiency with the MB concentration reduced as much as 100% in 240 min. Fig. 7 shows that the degradation kinetics of MB over the 0.3ZnO:0.7$SnO_2$ photocatalysts annealed at 400, 600, 700 and 800 °C. It shows that the photocatalytic activity of the 0.3ZnO:0.7$SnO_2$ photocatalyst increased when the annealed temperature was increased from 400 to 800 °C. To explore the advantage of 0.3ZnO:0.7$SnO_2$ molar ratio and its applicability, reuse cycles of new photocatalysts were tested for photodegradation of MB (Fig. 8). The recycling tests demonstrated that a photocatalyst with 0.3ZnO:0.7$SnO_2$ molar ratio was quite stable during that liquid–solid

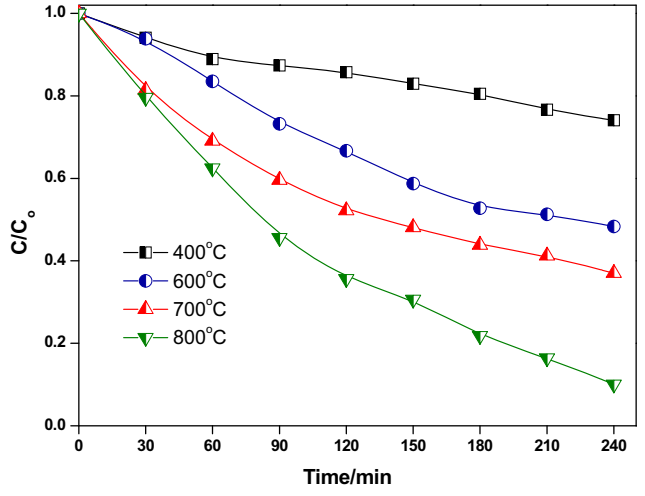


**Figure 7** Photocatalytic decolorization kinetics of MB using 0.3ZnO:0.7$SnO_2$ molar ratio photocatalysts annealed at different temperatures 400, 600, 700 and 800 °C. (MB concentration [$10^{-5}$ M], volume 250 ml.)

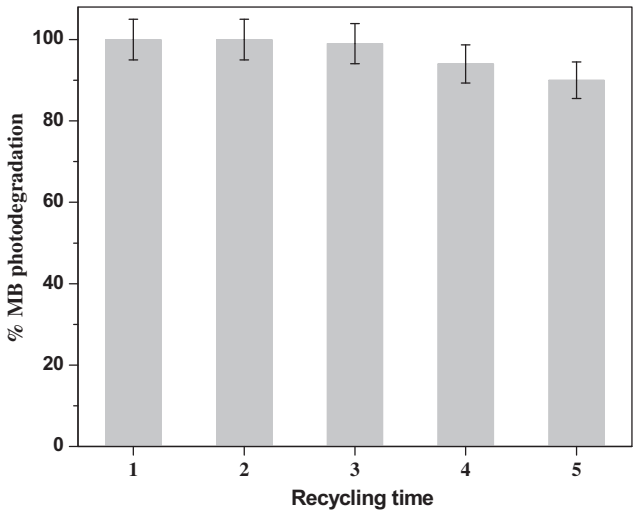


**Figure 8** Repeated cycles up to 5 times of photodegradation of MB over 0.3ZnO:0.7$SnO_2$ molar ratio photocatalysts under UV lights. (MB concentration [$10^{-5}$ M], volume 250 ml.)

heterogeneous photocatalysis since no decrease in activity in the first three cycles was observed. However, the photocatalytic activity was decreased to 90% after five cycles. In general, ZnO/$SnO_2$ nanocomposites are stable and can be recycled with a slight loss of their photochemical activity.

## 4. Conclusion

ZnO doped $SnO_2$ have been successfully synthesized by the solvothermal method using methanol as organic solvent. The lattice parameter, crystallite size, and unit cell volume were increased with increasing of the Zn substitution molar ratios. However, the band gap was decreased with increasing of the Zn substitution. The highest band energy was 3.75 eV for undoped $SnO_2$ whereas the lowest band energy was 3.33 eV at 0.3ZnO:0.7$SnO_2$ molar ratio. The results indicated that $Zn^{2+}$ doping at 0.3ZnO:0.7$SnO_2$ molar ratio showed the highest photocatalytic activity for the MB photodegradation. The recycling tests demonstrated that a 0.3ZnO:0.7$SnO_2$ molar ratio was quite stable during liquid–solid heterogeneous photocatalysis since no decrease in activity in the first three cycles was observed.

## References


Anandan, K., Rajendran, V., 2010. Size controlled synthesis of $SnO_2$ nanoparticles: facile solvothermal process. J. Non-Oxide Glasses 2, 83–89.

Borges, P.D., Scolfaro, L.M.R., Alves, W.L., Dasilvajr, E.F., 2010. DFT study of the electronic, vibrational, and optical properties of $SnO_2$. Theor. Chem. Acc. 126, 39–44.

Brokken-Zijp, J.C.M., Van Asselen, O.L.J., Kleinjan, W.E., Van de Belt, R., 2011. Photocatalytic properties of tin oxide and antimony-doped tin oxide nanoparticles. J. Nanotechnol. 2011, 15.

Broussous, L., Santilli, C.V., Pulcinelli, S.H., Craievich, A.F., 2002. SAXS study of formation and growth of tin oxide nanoparticles in the presence of complexing ligands. J. Phys. Chem. B 106, 2855–2860.

Dodd, A., McKinley, A., Saunders, M., Tsuzuki, T., 2006. Mechanochemical synthesis of nanocrystalline $SnO_2$–ZnO photocatalysts. Nanotechnology 17, 692–698.

Dutta, K., De, S.K., 2007. Optical and nonlinear electrical properties of $SnO_2$–polyaniline nanocomposites. Mater. Lett. 61, 4967–4971.

Fang, L.M., Zu, X.T., Li, Z.J., Zhu, S., Liu, C.M., Wang, L.M., Gao, F., 2008. Microstructure and luminescence properties of Co-doped $SnO_2$ nanoparticles synthesized by hydrothermal method. J. Mater. Sci. Mater. Electron. 19, 868–874.

Firooz, A.A., Mahjoub, A.R., Khodadadi, A.A., 2008. Preparation of $SnO_2$ nanoparticles and nanorods by using a hydrothermal method at low temperature. Mater. Lett. 62, 1789–1792.

Fouad, O.A., Ismail, A.A., Zaki, Z.I., Mohamed, R.M., 2006. Zinc oxide thin films prepared by thermal evaporation deposition and its photocatalytic activity. Appl. Catal. B 62, 144.

Fujishima, A., Rao, T.N., Tryk, D.A., 2000. Titanium dioxide photocatalysis. J. Photochem. Photobiol. C 1, 1.

Gu, F., Wang, S.F., Lu, M.K., Qi, Y.X., Zhou, G.J., Xu, D., Yuan, D.R., 2003. Luminescent properties of $Mn^{2+}$-doped $SnO_2$ nanoparticles. Inorg. Chem. Commun. 6, 882–885.

He, J.H., Wu, T.H., Hsin, C.L., Li, K.M., Chen, L.J., Chueh, Y.L., Chou, L.J., Wang, Z.L., 2006. Beaklike $SnO_2$ nanorods with strong photoluminescent and field-emission properties. Small 2, 116–120.

Hoffmann, M.R., Martin, S.T., Choi, W., Bahnemann, D.W., 1995. Environmental application of semiconductor photocatalysis. Chem. Rev. 95, 69.

Huh, M., Kim, S., Ahn, J., Park, J., Kim, B., 1999. Oxidation of nanophase tin particles. Nanostruct. Mater. 11, 211–220.

Ismail, A.A., 2008. Single-step synthesis of a highly active photocatalyst for oxidation of trichloroethylene. Appl. Catal. B 85, 33–39.

Ismail, A.A., Bahnemann, D.W., 2011. Mesoporous titania photocatalysts: preparation, characterization and reaction mechanisms. J. Mater. Chem. 21, 11686–11707.

Ismail, A.A., Bouzid, H., 2013. Synthesis of mesoporous $CeO_2$/$TiO_2$ thin films for self-cleaning applications. J. Colloid Interface Sci. 404, 127–134.

Ismail, A.A., El-Midany, A.A., Abel-Aal, E.A., El-Shall, H., 2005. Application of statistical design strategies to optimize the preparation of ZnO nanoparticles via hydrothermal technique. Mater. Lett. 59, 1924–1928.

Ismail, A.A., Bahnemann, D.W., Robben, L., Wark, M., 2010. Palladium doped porous titania photocatalysts: impact of mesoporous order and crystallinity. Chem. Mater. 22, 108–116.

Ismail, A.A., Bahnemann, D.W., Al Sayari, S.A., 2012. Synthesis and photocatalytic properties of nanocrystalline Au, Pd and Pt photodeposited onto mesoporous $RuO_2$–$TiO_2$ nanocomposites. Appl. Catal. A 431–432, 62–68.

Kormann, C., Bahnemann, D.W., Hoffmann, M.R., 1991. Photolysis of chloroform and other organic molecules in aqueous $TiO_2$ suspensions. Environ. Sci. Technol. 25, 494–500.

Kostedt, W.L., Ismail, A.A., Mazyck, D.W., 2008. Impact of heat treatment and composition of ZnO–$TiO_2$ nanoparticles for photocatalytic oxidation of an azo dye. Ind. Eng. Chem. Res. 47, 1483–1487.

Kotsikau, D., Ivanovskaya, M., Orlik, D., Falasconi, M., 2004. Gas-sensitive properties of thin and thick film sensors based on $Fe_2O_3$–$SnO_2$ nanocomposites. Sens. Actuators B 101, 199–206.

Lin, C.-C., Chiang, Y.-J., 2012. Preparation of coupled ZnO/$SnO_2$ photocatalysts using a rotating packed bed. Chem. Eng. J. 181–182, 196–205.

Mahamoud, M.H.H., Ismail, A.A., Sanad, M.S.S., 2012. Developing a cost-effective synthesis of iron oxide doped titania photocatalysts loaded with palladium, platinum or silver nanoparticles. Chem. Eng. J. 187, 96–103.

Mills, A., Lee, S.K., 2002. A web-based overview of semiconductor photochemistry-based current commercial applications. J. Photochem. Photobiol. 152, 233–247.

Monredon, S., Cellot, A., Ribot, F., Sanchez, C., Armelao, L., Gueneau, L., Delattre, L., 2002. Synthesis and characterization of crystalline tin oxide nanoparticles. J. Mater. Chem. 12, 2396–2400.

Pal, B., Hata, T., Goto, K., Nogami, G., 2001. Photocatalytic degradation of *o*-cresol sensitized by iron–titania binary photocatalysts. J. Mol. Catal. A 169, 147.

Rumyantseva, M.N., Kovalenko, V.V., Gaskov, A.M., Pagnier, T., Machon, D., Arbiol, J., Morante, J.R., 2005. Nanocomposites $SnO_2/Fe_2O_3$: wet chemical synthesis and nanostructure characterization. Sens. Actuators B 109, 64–74.

Sathyaseelan, B., Senthilnathan, K., Alagesan, T., Jayavel, R., Sivakumar, K., 2010. A study on structural and optical properties of Mn- and co-doped $SnO_2$ nanocrystallites. Mater. Chem. Phys. 124, 1046–1050.

Sharma, A., Varshney, M., Kumar, S., Verma, K.D., Kumar, R., 2011. Magnetic properties of Fe and Ni doped $SnO_2$ nanoparticles. Nanomater. Nanotechnol. 1, 29–33.

Suh, S., Zhang, Z., Chu, W., Hoffman, D.M., 1999. Atmospheric-pressure chemical vapor deposition of fluorine-doped tin oxide thin films. Thin Solid Films 345, 240–243.

Tauc, J., Grigorovici, R., Vanuc, A., 1966. Optical properties and electronic structure of amorphous germanium. Phys. Status Solidi, 15627.

Tennakone, K., Bandara, J., 2001. Photocatalytic activity of dye-sensitized tin(IV) oxide nanocrystalline particles attached to zinc oxide particles: long distance electron transfer via ballistic transport of electrons across nanocrystallites. Appl. Catal. A 208, 335.

Vinodgopal, K., Bedja, I., Kamat, P.V., 1996. Nanostructured semiconductor films for photocatalysis photoelectron–chemical behavior of $SnO_2/TiO_2$ composite systems and its role in photocatalytic degradation of a textile azo dye. Chem. Mater. 8, 2180.

Wang, C., Xu, B.Q., Wang, X., Zhao, J., 2005. Preparation and photocatalytic activity of $ZnO/TiO_2/SnO_2$ mixture. J. Solid State Chem. 178, 3500–3506.

Yu, J.C., Lin, J., Kwok, R.M., 1998. $Ti_{1-x}Zr_xO_2$ solid solutions for the photocatalytic degradation of acetone in air. J. Phys. Chem. B 102, 5094.

Yuan, H., Xu, J., 2010. Preparation, characterization and photocatalytic activity of nanometer $SnO_2$. Int. J. Chem. Eng. Appl. 1, 3.

Zhang, M., Sheng, G., Fu, J., An, T., Wang, X., Hu, X., 2005. Novel preparation of nanosized $ZnO–SnO_2$ with high photocatalytic activity by homogeneous co-precipitation method. Mater. Lett. 59, 364–3644.

Zheng, Y., Wang, C., Mao, Z., Wang, N., 2007. Preparation of nanometer-sized $SnO_2$ by the fusion method. Mater. Lett. 61, 1205–1209.

Zheng, L., Zheng, Y., Chen, C., Zhan, Y., Lin, X., Zheng, Q., Wei, K., Zhu, J., 2009. Network structured $SnO_2/ZnO$ heterojunction nanocatalyst with high photocatalytic activity. Inorg. Chem. 48, 1819–1825.

Zhong, G., Liu, M., 1999. Preparation of nanostructured tin oxide using a sol–gel process based on tin tetrachloride and ethylene glycol. J. Mater. Sci. 34, 3213–3219.